

We are IntechOpen, the world's leading publisher of Open Access books Built by scientists, for scientists

6,900

Open access books available

186,000

International authors and editors

200M

Downloads

Our authors are among the

154

Countries delivered to

TOP 1%

most cited scientists

12.2%

Contributors from top 500 universities



WEB OF SCIENCE™

Selection of our books indexed in the Book Citation Index
in Web of Science™ Core Collection (BKCI)

Interested in publishing with us?
Contact book.department@intechopen.com

Numbers displayed above are based on latest data collected.
For more information visit www.intechopen.com



Visualization Methods for Numerical Astrophysics

Werner Bengert^{1,2}, Markus Haider¹, Harald Höller¹, Dominik Steinhauser¹,
Josef Stöckl¹, Biagio Cosenza¹ and Marcel Ritter¹

¹*Department of Astro- and Particle Physics, Distributed and Parallel Systems Group,
University of Innsbruck, Innsbruck*

²*Center for Computation & Technology at Louisiana State University, Baton Rouge*

¹*Austria*

²*USA*

1. Introduction

Numerical simulations of astrophysical processes and subsequent predictions are an important complement to observational astronomy. With increasing computational performance available the demands on accuracy and functionality of the simulations grow steadily, leading to increasing amounts of complex data sets requiring three-dimensional visualization for proper analysis. Modern graphics hardware provides suitable rendering technology, however, many visually impressive approaches used in computer games, for instance, do not immediately transport over to application upon scientific data sets since priorities are different. Specific software for scientific visualization of astrophysical data does not necessarily need to provide photo-realistic rendering, but should rather be able to comprehensively display all features of a data set. False-color imaging has long been an established approach in observational astronomy. For three-dimensional time-dependent data sets the optional parameter space is even larger. As similar requirements occur in other scientific domains beyond astrophysics, data visualization benefits extraordinarily well from interdisciplinary approaches, for instance describing curved space in general relativity is similar to diffusion tensor fields occurring in magneto-resonance imaging in medical visualization (Benger et al., 2006).

Visualization of numerical astrophysics faces certain challenges because of the different data types involved together. For instance, a typical visualization data set may involve both particle-based and volumetric data, thus requiring complex techniques to handle transparency, see e.g. Kaehler et al. (2007).

Interdisciplinary approaches face various difficulties, starting with incompatibilities of the data format and data model (Benger, 2009). Common use is to provide specific solutions to specific problems. Unifying approaches to cover various needs under one denominator are rare, but essential in the longer term (Dougherty et al., 2009). In this article we will review a systematic approach for modeling and visualization of data sets across scientific disciplines, demonstrating this approach upon a set of state-of-the art astrophysical simulations.

2. Open issues in numerical astrophysics

The demand for sophisticated numerical simulations and hence for high performance visualization is somewhat exceptional in the field of astrophysics. Other than related disciplines, astrophysical research is very limited in the feasibility to conduct controlled experiments with their objects of interest. Experimental data and deduced knowledge is mainly gained from extensive observational studies. However they generally lack two important pieces of information: Due to the vast time scales of astrophysical processes (typically $10^6 - 10^9$ years), imaging comes practically without any data on temporal evolution, since even a decade of astronomical observation is nothing but a snatch on these scales. Moreover, we always find entirely two dimensional spatial information in astrophysical images, since - especially for extragalactic objects - the viewing angle between the observatory and the astrophysical object is fixed. Hence, scientific insight to the evolution and development of astrophysical targets comes from comprehensive statistical analysis of a large number of single observations that are interlinked to a big picture.

From a purely theoretical point of view, the physics that governs astrophysical processes and objects are very well known; a multitude of systems and configurations are described with concepts from hydrodynamics coupled with gravitation, radiation and magnetism. Mathematically, radiation hydrodynamics (RHD) and magnetohydrodynamics (MHD) are systems of coupled nonlinear partial differential equations. The necessity for enormous computational efforts lies in the nonlinearity of the equations on the one hand and the diversity of time- and spatial scales that are involved and to be resolved on the other hand. Supercomputing has thus become a major driver for research in astrophysics and even has opened entirely new fields that defy astronomical observations at the present state of technology. In the following two sections we want to present two case studies of astrophysical numerical simulations where data examinations benefit immensely from visualization techniques.

2.1 Galaxy clusters

Groups and clusters of galaxies have formed cosmologically *recently* in the hierarchical structure formation process of the universe. They are the largest gravitationally bound objects known and were mainly built during the last four billion (10^9) years by successive merging of galaxies, a picture that is supported both by observations (White & Frenk, 1991) as well as simulations (Bertschinger, 1998). The common understanding of cosmological structure formation is based on the so called *concordance model* (Ostriker & Steinhardt, 1995), which assumes hypothetical massive particles in the form of cold dark matter (CDM), a collisionless species of material that exclusively interacts gravitationally. In this CDM model, primordial fluctuations briefly after the big bang acted as gravitational potential seeds for slightly inhomogeneous mass accumulations that were not felt by normal baryonic matter until the universe had cooled down substantially. The length scales and amplitudes of these anisotropies can be observed in the cosmic microwave background (de Oliveira-Costa et al., 2004) and are used for the generation of initial conditions for CDM simulations on cosmological scales.

2.1.1 Simulation setup

For initial conditions we are using COSMICS (Bertschinger, 1995), a package that generates appropriate Gaussian random initial conditions with the feasibility to enforce statistical overdensities of dark and baryonic matter at designated places in the domain. This way, groups and clusters of dark matter halos evolve naturally within a N-body simulation of collisionless CDM. In our setup we model dark matter particles with the N-body implementation of GADGET-2 (Springel, 2005). This sophisticated parallelized tree-code is applied at resolutions of $128^3 - 512^3$ particles in comoving volumes of 40Mpc/h which produces up to > 2 TB of binary data for > 130 million particles traced. We are primarily interested in secondary processes (rather than structure formation itself) that affect the baryonic matter fraction of such as the formation of actual galaxies within dark matter halos and their interaction with the surrounding gas, the so called intra cluster medium (ICM). Our premier research topic deals with the enrichment of this ICM with chemical elements that are produced in stars and transported to the intra cluster gas via a number of distinct mechanisms. One main challenge in such simulations is a proper modeling of the astrophysical processes on the wide range of spatial and temporal scales that are at play. While we are interested in gas dynamics up to several Mpc radius from the cluster center, those mechanisms that cause the enrichment of the ICM with heavier elements occur on practically stellar dimensions ($< \text{pc}$), such as stellar winds, the loss of gaseous envelopes at the AGB phase of stellar evolution and supernovae explosions. Even with the most advanced technical facilities imaginable today we would still be far away from being able to resolve such a wide range of scales consistently.

In order to overcome this dilemma, semi-analytical galaxy formation models (SAM) are introduced. These SAMs deduce characteristic galactic quantities by a recipe based on the merger history of the dark matter halos that were simulated beforehand. In other words, the SAM assigns collective quantities such as total gas mass, angular momentum, starformation rate in the galaxies etc. to the halos regarding their merger history by observationally motivated, heuristic formulae and prescriptions. We use our own semi-analytical model (van Kampen et al., 1999) while there is also a relevant publicly available open source project called Galacticus (Benson, 2010). On top of all specified preliminary simulations there is a hydrodynamical grid-code with PPM Riemann solver that treats the intra cluster medium on the gravitational background of the dark matter simulation. The output from the SAM provides for two main contributions to ICM enrichment with chemical elements, namely ram-pressure stripping and galactic winds (see section 2.1.2), which are used as input for the hydrodynamical simulation. The number of independent points in computation is $11/8 \cdot 128^3$ up to $11/8 \cdot 512^3$ due to the fact that we apply four nested grids each with doubling resolution. The galaxy cluster is forming in the domain center of the hydrodynamical simulation which captures a smaller volume than the CDM simulation in order to have adequate boundary conditions for the gas flows (mainly inflow). All of the simulations are conducted on a non-steady scale, the aforementioned comoving volume of the cosmic expansion. The physical variables are scaled accordingly to this expansion, in cosmology sometimes also called the *Hubble flow*.

2.1.2 Metal enrichment by ram-pressure stripping and galactic winds

The chemical evolution of the universe is quite well understood in principle. The theory of primordial nucleosynthesis provides abundances that fill the early universe merely with hydrogen and helium homogeneously. However we know that today's universe is high in

heavier elements, such as carbon, silicon, oxygen etc. Furthermore we know that these heavy elements (in astrophysics also called metals) have to be synthesized in stars but the question remains: How are they transported into the ICM of a galaxy group or a galaxy cluster where we can observe them (Blanton et al., 2003; Lovisari et al., 2009)?

There are two main astrophysical mechanisms that enrich the intra cluster medium, namely ram-pressure stripping and galactic winds while the latter is to be understood as collective of numerous distinct astronomical processes. Ram-pressure is the force a galactic plane of gas experiences while falling towards the center of a cluster due to the surrounding ICM as described in section 2.2. Ram-pressure stripping occurs whenever a certain pressure threshold is reached, and leads to the separation of the galaxy's planar gas from the stellar component of stars in the disk. Its contribution to metal enrichment in galaxy clusters is mainly influenced by the density of the ICM which naturally shows a gradient towards the cluster center. Also the in-falling velocities of the galaxies increase towards the main potential well in the center. Hence, ram-pressure stripping is primarily governed by circumstances of kinematics and the spatial distribution of the galaxies (Domainko et al., 2008). On the other hand, galactic winds are dominantly affected by the factors of galactic evolution such as the history of merger events and subsequent star-burst phases which lead to enormous galactic winds due to temporarily concentrated collective supernovae explosions (Finoguenov et al., 2000). Generally, galactic winds are driven by the star formation rate which is in principle higher in early times of cluster formation since merging events occur much more frequently. Such disturbances trigger density fluctuations in the gas which then leads to increased star formation.

We are interested in the efficiency of different transport processes in enriching the ICM and in the spatial distribution of metal abundances in the cluster at a certain epoch of evolution. Due to the complexity of the involved physical processes and the richness of our data, we are keen to visualize the manifold parameter space both preferably exhaustive and as clearly as possible, which will be discussed exemplary in section 4.1.

2.2 Ram-pressure stripping of disk galaxies

As described in section 2.1, galaxy clusters consist of dark matter, galaxies and a hot, thin gas, the ICM. These clusters of galaxies have been formed through the hierarchical structure formation process from dark matter and primordial gas. Part of the primordial gas, the ICM, can be observed by X-ray observations. This plasma, even though it is very hot ($\sim 10^8 K$) and thin ($10^{-29} - 10^{-26} \text{ g cm}^{-3}$), exerts a pressure on the inter-stellar medium (ISM). According to (Gunn & Gott, 1972), the ISM is stripped if this ram pressure exceeds the gravitational restoring force. Moreover, ram pressure compresses the gas in the spiral arms of the galaxy and enhances the star formation within the galaxy. External pressure of the ICM also causes the formation of dense gas knots where lots of new stars are formed (e.g. (Hester et al., 2010)). Yet it is unclear and matter of research how efficient these processes are with uncertainties being mainly mixing of different gas phases and instabilities.

2.2.1 Simulation setup

To simulate ram-pressure stripping of a galaxy, we use the N-body/hydrodynamic simulation code GADGET-2 (Springel, 2005). The N-body part treats the collisionless dynamics of dark-matter and stars. To this end, GADGET-2 uses a sophisticated tree code (as first

introduced by Barnes & Hut, 1986) and treePM code respectively to calculate the gravitational force. The gas of the galaxies and the ICM are treated hydrodynamically via smoothed particle hydrodynamics (SPH, see Gingold & Monaghan, 1977; Lucy, 1977)). Furthermore, our special version of GADGET-2 includes radiative cooling according to (Katz et al., 1996) and a recipe for star formation, stellar feedback and galactic winds from (Springel & Hernquist, 2003) because we are mainly interested in the influence of ram-pressure stripping on the star formation. As the resolution in our simulations is far too low to resolve gas clouds forming single stars, the star formation in the ISM is described in a statistical manner. The continuous distribution of the ISM is represented by SPH particles, holding spatially averaged hydrodynamic quantities, the star formation is calculated for each such particle. The gas mass is divided into two gas phases, hot ambient medium used for hydrodynamic computations and cold gas clouds which form new stars on a characteristic time scale when a density threshold is exceeded. During star formation, at the same time, a fraction of 10 % according to a Salpeter IMF (Salpeter initial mass function, see Salpeter, 1955) is immediately released to the hot ambient medium due to supernovae from massive stars exceeding $8 M_{\odot}$. The inclusion of the cooling of hot ambient medium leads to the growth of the cold gas clouds making star formation self regulating.

To simulate ram-pressure stripping of disk galaxies, we need a model galaxy as well as a way to simulate the ICM, interacting with the model galaxy. Model galaxies include the ISM, the stellar disk, a bulge and dark matter. For the stellar and gaseous component a disk with exponentially decreasing density along the radius is used whereas for the bulge and the dark-matter halo a NFW profile (Navarro et al., 1996) is applied. Consequently, the distribution and velocity of the particles are set according to (Mo et al., 1998). To avoid numerical artifacts and to get a realistic model, we evolve the galaxies in isolation for 1 billion years. Thereafter, the star formation rate has settled and spiral arms are forming in the disk.

Finally, the model galaxies interact with the ICM. For that purpose, the setup described in Kapferer et al. (2009) and Kronberger et al. (2008) is used. The idea is to simulate the effect of a wind tunnel. The galaxy is moving instead of the wind in our setup, leading to the same result. We fill a cube with gas particles to represent the ICM. To keep the gas density stable over time, periodic boundary conditions are imposed. To avoid numerical artifacts due to the SPH scheme, the same gas mass-resolution as for the ISM has to be used. Since only cubic simulation domains are supported and a side-length of at least 800 kpc for the cube is needed, a huge amount of particles would be necessary. To avoid lowering the resolution in the ISM, just a cuboid of gas particles with the required resolution is built up where the model galaxy flies through. The rest of the cube is filled with gas particles having a 100 times lower mass resolution. Anyway, the same gas density is used. With this configuration, the density of the wind-tunnel changes only by 4 % over a simulation time of 800 million years. We evaluate the results, finally, by removing the ICM particles from the data to investigate the morphology of the gas and stellar disk as well as the influence of ram-pressure stripping on the star formation rate.

3. Visualization methodology

In many visualization systems solutions to a particular problem are based on specific data structures. Such diverse approaches are sensitive to the growing demands of new datasets, as such may likely require design changes leading to incompatibilities within the same application as well as among older and younger data sets. Even worse, an extensive set of

specific solutions effects the learning curve of both the application developer and end-user of the visualization system since each solution has to be learned anew on a case-by-case basis. Our approach, based on the Vish Visualization Shell (Benger et al., 2007), contrasts such ad-hoc approaches on the design level by routing all data structures and visualization methods based on them through a common denominator, providing a systematic approach for modeling data and visualizing them. While this concrete data structure is limited in applicability to a certain type of data, this class of data types is broad enough to address most cases occurring in scientific visualization. This data model will be reviewed in this section and discussed for its applicability specifically to data sets from astrophysical simulations.

3.1 Using a common data model

Expressing all types of data occurring in astrophysical simulations within the same data organization framework is the first step towards a systematic approach contrasting ad-hoc visualization on case-by-case basis. No commonly agreed solution exist yet, but an approach based on the mathematics of fiber bundles has been proposed early by (Butler & Pendley, 1989). Inspired by its successful implementation in the OpenDX data explorer (Treinish, 1997), the data model has been advanced to cast data into a hierarchy of six levels (Benger, 2004). This skeleton forms the basis for visualizing data in a very generic and reusable way (Benger, 2008).

3.1.1 Mathematical background

The central idea is to organize data by their mathematical commonalities, following the theories of topology, differential geometry, and geometric algebra (Hestenes, 1999). The model is based on the assumption that data for scientific visualization can be organized as a fiber bundle, which considers a total space E as being constructed from a base space B and a fiber space F such that locally $E = B \times F$. The base space in this context is described by a discretized manifold, which in topology is modeled via a *CW-complex* as a hierarchical set of spaces, the so-called k -skeletons, each of them describing vertices, edges, faces, cells of some spatial domain (see Benger et al., 2011, for a more detailed review). Differential geometry introduces charts as mappings from manifolds to real numbers, allowing to represent physical quantities given at each point of the underlying manifold numerically in one or more coordinate systems. Having the choice of alternative numerical representations of the same physical quantity is essential for computational accuracy since not all coordinate systems are equivalently suited for a particular problem. However, the numerical representation of some quantity is frequently confused with the object itself, though differential geometry demonstrates that objects with same numerical representation (for instance, three numbers) have different mathematical properties (e.g. covariant and contra-variant vectors). Not many data models (and file formats) support expressing such distinctions as required by accurate treatment of differential geometry. One step further is even the consideration of Geometric Algebra (Hestenes, 1999), which intends to unify various branches of mathematics itself through a common treatment. It is thus a natural complement to be considered in a data model (Benger et al., 2010).

3.1.2 Conceptual data organization

In the model used for our work data are cast into a hierarchy of seven levels. These levels are:

1. **Slice** - bundles all data by their parameter space such as physical time
2. **Grid** - bundles all data related to a geometric entity
3. **Skeleton** - bundles all data related to a topological property
4. **Representation** - bundles all data related to a specific coordinate system
5. **Field** - contains data representing a physical quantity
6. **Fragment** - contains a subset of a data field
7. **Component** - contains a component of a multi-valued field

From these seven levels only two are exposed to the end-user: the **Grid** and the **Field**; the remaining levels serve to internally describe the mathematical properties of the data. The two last levels, **Fragment** and **Component**, are optional, and used to express practical extensions beneficial to domain decomposition in HPC computations and different memory layouts (Benger, 2008). Actual data in the form of numerical arrays reside only in the last level of this hierarchy. Each of these arrays is accessed via a path through this hierarchy, similar to a file in a filesystem. This path defines the semantics of the given data values and the existence of entries in the hierarchy defines the properties of the entire data set. For instance, diagram (1) demonstrates how the coordinates of a particle data set describing dark matter at a time 3.4Gy are modeled using a Cartesian chart (" $/$ " denotes the "root" node which bundles all data):

$$/ \xrightarrow{\text{Slice}} 3.4\text{Gy} \xrightarrow{\text{Grid}} \text{Dark Matter} \xrightarrow{\text{Skeleton}} \text{Vertices} \xrightarrow{\text{Representation}} \text{Cartesian Chart} \xrightarrow{\text{Field}} \text{Positions} \quad (1)$$

Similarly arbitrary fields such as velocity of the particles can be added to the data:

$$/ \xrightarrow{\text{Slice}} 3.4\text{Gy} \xrightarrow{\text{Grid}} \text{Dark Matter} \xrightarrow{\text{Skeleton}} \text{Vertices} \xrightarrow{\text{Representation}} \text{Cartesian Chart} \xrightarrow{\text{Field}} \text{Velocity} \quad (2)$$

The *Skeleton* level carries a set of topological invariants described by integer values: *dimensionality*, *index depth* and *refinement*. Hereby *index depth* denotes the "dereference" information of a Skeleton, similar to a pointer indirection in C, allowing to build agglomerations of points: Vertices are assigned index depth zero, k-cells constructed from vertices are index depth one, complexes of cells are index depth two and so forth. The *dimensionality* is an intrinsic property of a topological space, which is uniquely defined by its neighborhood information. This neighborhood information could be explicitly specified by providing a map from each element to its neighbors (such as required for a particle set), or implicitly in case of a structured data set given by an n -dimensional array. Such a gridded data set (a regular grid) is described by two entries, one defining the coordinate information (physical coordinates), the second one the actual data, for instance a density field:

$$/ \rightarrow 3.4\text{Gy} \rightarrow \text{Dark Matter} \rightarrow \text{Vertices:}32 \times 32 \times 32 \rightarrow \text{Cartesian Chart} \rightarrow \text{Positions} \quad (3)$$

$$/ \rightarrow 3.4\text{Gy} \rightarrow \text{Dark Matter} \rightarrow \text{Vertices:}32 \times 32 \times 32 \rightarrow \text{Cartesian Chart} \rightarrow \text{Density} \quad (4)$$

The positions may be given explicitly at each point (curvilinear grid), via a tensor product of one-dimensional arrays (rectilinear grid) or by specifying just the bounding box of a uniform grid. This infrastructure allows to naturally exploit commonalities among data sets describing particle sets and uniform grids as the mere difference is the dimensionality of the skeleton describing the vertices. A specific visualization algorithm may or may not consider this property, but in any case will be based on the same data management functions. In a

similar manner as distinguishing particle sets and uniform (or curvilinear, rectilinear) grids within the same framework more complex and other data types can be built, for instance by adding refinement levels as additional Skeletons (adaptive mesh refinement), or utilizing the Fragment level to specify a distribution of a data set by many blocks (multiblock data) instead of one contiguous data volume.

3.2 Visualization on the fiber bundle

3.3 Base space

The base space of a data set refers to the topological properties of how data are given in space, in particular if (and what kind of) neighborhood information among data points is known. For instance, for a particle set we might not know such neighborhood information and we may thus consider it to be “zero-dimensional” even though these particles may be embedded in some two- or three-dimensional space. This embedding would allow to construct neighborhood information (e.g. via triangulation), but such is secondary information as it does not come with the data set per se.

3.3.1 Zero-dimensional base space

Display of a point sets’ coordinates is the most common denominator across all data types and can be done for any data set providing a global coordinate system (which is not necessarily the case for general relativistic data where a curved spacetime does not necessarily exhibit a global coordinate system, but must rather be described by coordinate patches - “fragments” in the data model).

Splatting (Westover, 1990) is a technique for displaying smooth volumetric information on a point set, appropriate both for particle sets as well as for unstructured and structured grids. In its basic implementation it draws billboards with a point spread function at each coordinate location, a technique which is well supported by graphics hardware. Using a Gaussian intensity function is a frequent choice for the point spread function, but other functions have their merits as well. We use the same spline kernel (Monaghan & Lattanzio, 1985) as point spread function for the visualization as is used in the SPH simulations performed by GADGET-2 (Springel, 2005), which has the advantage of vanishing at the boundaries of the finite billboard geometry (in contrast to a Gaussian function which extends to infinity):

$$I(r) \propto \begin{cases} 1 - 6r^2 + 6r^3 & 0 \leq r \leq \frac{1}{2} \\ 2(1 - r)^3 & \frac{1}{2} < r < 1 \\ 0 & r \geq 1 \end{cases} \quad (5)$$

Here, r is the normalized radius per billboard (point splat) ranging from zero to one and $I(r)$ the intensity at each pixel. The size of the splat may be constant or scaled with a numerical value given at each point (for instance the mass of a galaxy’s stellar disc). This intensity function forms the basics for displaying scalar-, vector- and tensor fields given at each point. Point splatting is most effective when rendering the billboards transparently; this however turns out to be quite challenging, as will be discussed in section 3.5.

3.3.2 One-dimensional base space

In a one-dimensional base space each vertex has exactly two neighbors, described via a Skeleton of dimension one and index depth one for the “edges” of this data set. A sequence of edges is modeled by a Skeleton of index depth two, which defines a set of lines. It is described in the data model by three nodes:

$$/ \rightarrow 3.4Gy \rightarrow \text{Dark Matter} \rightarrow \text{Vertices} \rightarrow \text{Cartesian Chart} \rightarrow \text{Positions} \quad (6)$$

$$/ \rightarrow 3.4Gy \rightarrow \text{Dark Matter} \rightarrow \text{Edges} \rightarrow \text{Vertices} \rightarrow \text{Positions} \quad (7)$$

$$/ \rightarrow 3.4Gy \rightarrow \text{Dark Matter} \rightarrow \text{LineSet} \rightarrow \text{Edges} \rightarrow \text{Positions} \quad (8)$$

Hereby the edge and lineset information is just a collection of arrays of indices. In the context of astrophysical SPH simulations lines occur as trajectories of the involved particles, showing their evolution over time. Given a line we may explore intrinsic scalar (fig. 1) or vectorial (fig. 2) quantities such as the velocity, curvature (which is related to the acceleration) and torsion (which is related to the change of the acceleration), see e.g. (Benger & Ritter, 2010) for a discussion of line properties for visualization. Such may help verifying the dynamic model of the simulation and provide further insight to the dynamics.

Difficulties arise if the number of particles varies over time, for instance when considering mergers of galaxies. In such case a particle given at one time does not have a unique predecessor which leads to trajectories becoming non-manifolds where derivative operations are no longer defined. In the data model it is possible to model such topologies by providing explicit “future” and “past” skeletons that map the index of one particle at a time to the set of successors or predecessors. In order to provide this information, this topology has to be defined already in the previous simulation step, namely the link between the N-body simulation and the semi-analytical galaxy model as described in section 2.1.1. This intermediate step is realized via so called *halo finders* (Knebe et al., 2011) which identify gravitationally bound structures but often fail to represent a holistic merger tree with unique mappings over several time steps.

3.3.3 Two-dimensional base space

Surfaces introduce a Skeleton of dimension two and index depth one to the data model. Each element of this Skeleton describes a *face* element, which are triangles for a triangular surface. Such a Skeleton may co-exist with a line set Skeleton, thereby allowing to describe paths within a surface. Evolution surfaces tracing the dynamic behavior of some initial surface may be of interest, as well as iso-surfaces of a scalar quantity in a volume. For mere visual depiction of three-dimensional isolevels of a scalar field the explicit computation of isosurfaces (for instance using the marching cubes (Lorenson & Cline, n.d.) algorithm) is not required, modern graphics hardware allows to yield fast and even visually superior results via volume rendering with transparency set to “peaks” in the alpha channel, as will be discussed in the next section.

3.3.4 Three-dimensional base space

In the data model a three-dimensional base space is formally described by a one-dimensional Skeleton for the edges, a two-dimensional Skeleton for the faces and a three-dimensional Skeleton for the cells, extending the description of a two-dimensional base space by a

third dimension. In practice this full description is only required for irregular meshes, e.g. tetrahedral, hexahedral or mixed grids. For regular grids, where each vertex has eight neighbors these Skeletons can be omitted as specifying the number of vertices in each dimension is sufficient, allowing for extensions such as Adaptive Mesh Refinement (AMR) schemes (Berger & Olinger, 1984), multiblock and domain decomposition as well as curvilinear and rectilinear coordinates. Each of these properties can be independently introduced in the data layout, thus allowing all possible combinations (e.g. rectilinear multiblock, curvilinear AMR, etc.).

3.4 Fiber Space

3.4.1 One-dimensional fiber space

Scalar fields are an example of a one-dimensional fiber space as they provide one quantity per data point. Depending on the dimensionality of the base space, point splatting, colored lines or surface, or volume rendering are established techniques. Fig. 1 shows lines colored by intrinsic line quantities, norm of acceleration and torsion (change of acceleration). For

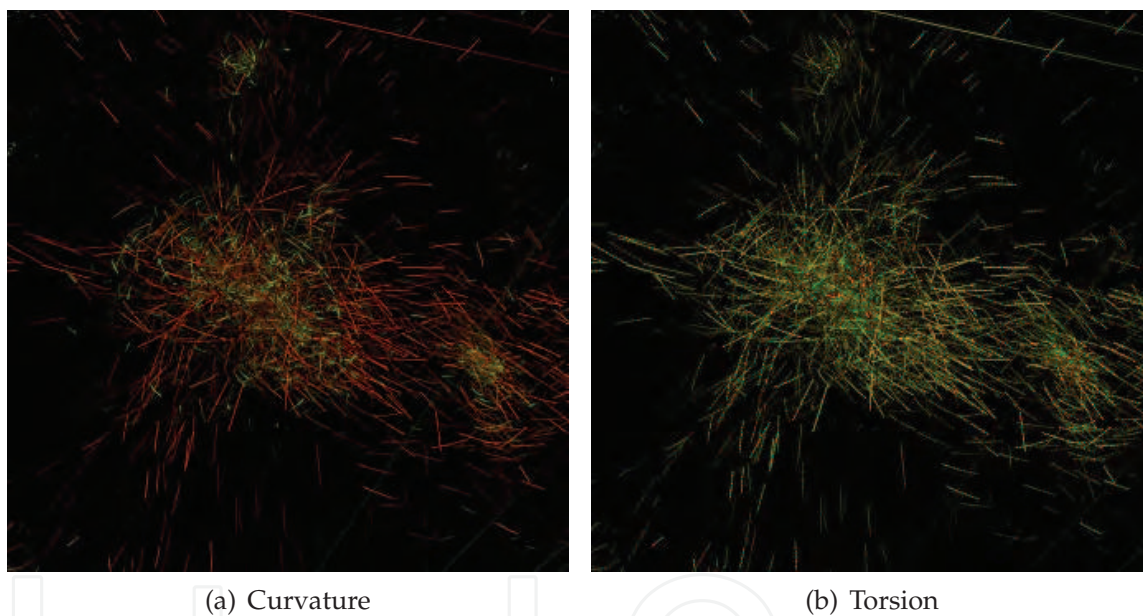


Fig. 1. Scalar properties of trajectories in the galaxy cluster.

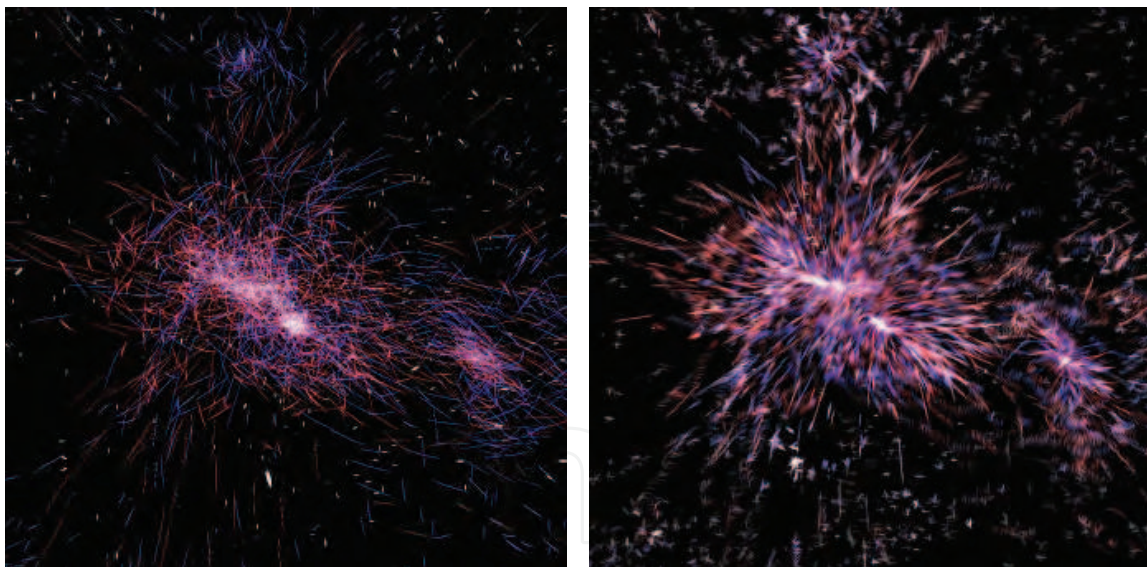
three-dimensional base spaces one of the most popular hardware-accelerated technique used to visualize one-dimensional Fiber Space (e.g. scalar field) is texture-based volume rendering. First introduced by Cullip & Neumann (1994), the basic idea is to approximate the volume rendering equation, eq. 13, by sampling the volume data using a stack of 2D textures, and to exploit graphics hardware capabilities to extract sets of slices from the volume. The volume rendering evaluation is then approximated by blending the textured slices in back-to-front order into the frame buffer. The high parallelism exposed by the pixel-processing unit during rasterization and the exploitation of bi- or trilinear interpolation capabilities of modern GPUs are the rationale behind of the success of this method. The technique has been further extended in several ways, e.g to support multiresolution representations of the volume data, to increase depth perception using shading (Stöckl et al., 2010) or to use an advanced optical model (see e.g. Kniss et al., 2002; Weiler et al., 2000).

3.4.2 Two-dimensional fiber space

It is often desirable to visualize the correlation of scalar fields, such as mass versus potential or other combinations. For particle sets (Benger, 2008) demonstrated the mapping of such scalar quantities to colorization, size and coordinate displacement of a splat-based representation. In situations where texture-based volume rendering can be used, the usual color-mapping algorithm can be extended to use the transparency values from another scalar field, thereby allowing to display two scalar fields at once in a volume (“dual volume rendering”, see section 4.2).

3.4.3 Three-dimensional fiber space

Vector fields constitute a three-dimensional fiber space. The intuitive way to visualize a vector field via arrows fails for massive amounts of data, in particular when given within a three-dimensional volume. The splatting technique for scalar fields can well be extended to incorporate directional information by using anisotropic splats (Crawfis & Max, 1993). In our work we extended this idea by adding a colorization mimicking doppler-shift such that the velocity component in view direction is mapped to red or blue. This technique of “Doppler Speckles” (Benger et al., 2009) is particularly effective for astrophysical data. It is of general usability independent from the dimensionality of the base space (as any splat-based technique) and allows to display e.g. the tangential vectors (fig. 2(a)) or the acceleration (fig. 2(b)) of galaxy trajectories.



(a) Galaxy Trajectory Velocity

(b) Galaxy Trajectory Acceleration

Fig. 2. Vectorial properties of galaxy cluster trajectories.

3.4.4 Higher-dimensional fiber space

Tensor fields extend the presented dimensionalities. Second order tensor fields are commonly used in computational physics, for example, to describe tension in continuum mechanics, viscosity in fluid dynamics, or space time curvature in numerical relativity. Direct and integration methods exist for visualization. An overview of tensor visualization can be found

in Bengert & Hege (2006). An integration method by computing geodesics is, for example, described in Ritter (2011). In figure 3 a direct splat based technique is applied, utilizing orientation, scaling, color and texture (presented in Bengert & Hege, 2003). Three shape factors linearity, planarity and sphericity, see Westin et al. (1997), are the basis for the appearance of a splat capturing the relationship of the eigenvalues. One dominant eigenvector results in high linearity, illustrated as green lines. Two dominant eigenvectors result in high planarity, illustrated as red plane. Three dominant eigenvectors result in high sphericity, illustrated through increased transparency, see fig. 3.

Fig. 3 shows tensor splats of the point distribution tensor illustrating geometrical properties of a point cloud. The point distribution tensor at a point i with position P_i is given by

$$T_{dist}(i) = \sum_{k=0}^{N-1} (P_k - P_i) \otimes (P_k - P_i)^t \quad (9)$$

where N is the number of points to consider.

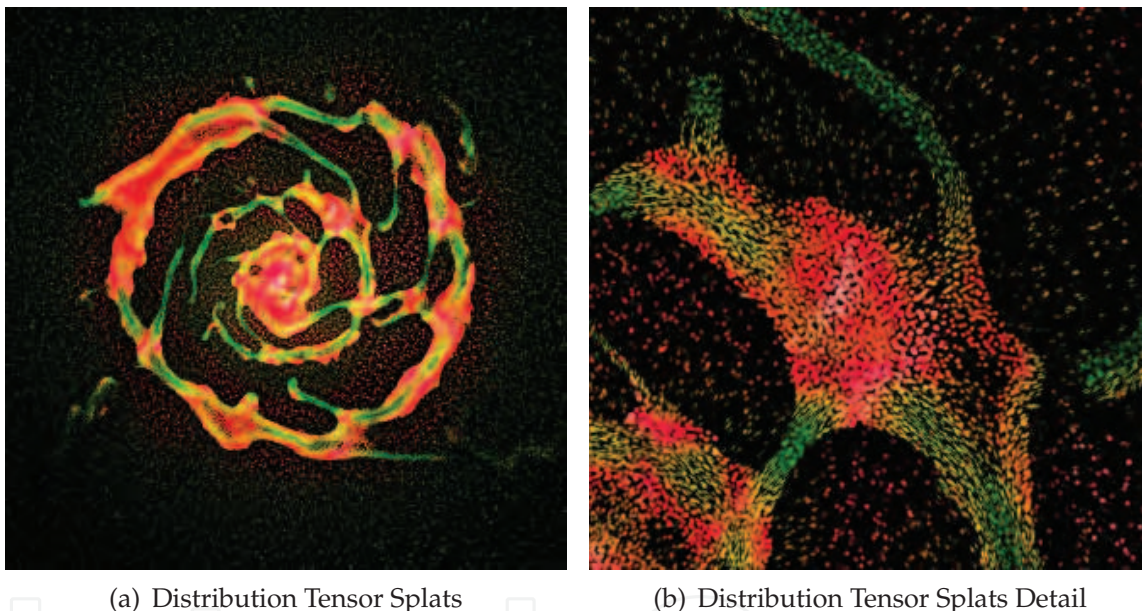


Fig. 3. Distribution tensor field of the RAM-pressure data set at $T = 0$ reveals geometric regions of linear, planar and volumetric structure. The neighborhood was chosen four times the SPH particle radius.

3.5 Fusing of methods via global transparency

Transparency has been enlisted as one of the five major challenges in interactive rendering and, more in general, of Computer Graphics (Andersson, 2010). As well as transparency, other physical phenomena such as absorption, emission and scattering processes identify energy transfers in the form of electromagnetic radiation. The equation of radiative transfer describes these interactions mathematically (Chandrasekhar, 1960) and in its simplest one-dimensional form it is known as

$$\frac{dI(s)}{ds} = \varepsilon(s) - \kappa(s)I(s) \quad (10)$$

where $\varepsilon(s)$ is the emissivity function (the source of light at each point along a sight path) and $\kappa(s)$ the extinction function (caused by light scattering or absorption). This differential equation has the general solution

$$I(s) = I(s_0)e^{-\int_{s_0}^s \kappa(\tilde{s})d\tilde{s}} + \int_{s_0}^s \mathcal{S}(\tilde{s})e^{-\int_{\tilde{s}}^s \kappa(\hat{s})d\hat{s}}d\tilde{s} \quad (11)$$

where $\mathcal{S}(s) := \varepsilon(s)/\kappa(s)$ is called the source function. For constant extinction $\kappa(s) = \text{const.}$ we can write the optical depth $\int_{s_0}^{s_1} \kappa(s)ds = \kappa(s_1 - s_0)$ leading to a simpler solution:

$$I(s) = I(s_0)e^{-\kappa(s-s_0)} + \int_{s_0}^s \mathcal{S}(\tilde{s})e^{-\kappa(s-\tilde{s})}d\tilde{s} \quad (12)$$

which for constant emissivity $\varepsilon(s) = \text{const.}$ (thus $\mathcal{S}(s) = \text{const.}$) reduces to the rendering equation used in computer graphics (Kajiya, 1986)

$$I(s) = I(s_0)e^{-\kappa(s-s_0)} + \mathcal{S} \int_{s_0}^s e^{-\kappa(s-\tilde{s})}d\tilde{s} = I(s_0) \underbrace{e^{-\kappa(s-s_0)}}_{=: \alpha} + \mathcal{S} (1 - \underbrace{e^{-\kappa(s-s_0)}}_{\alpha}) \quad (13)$$

$$= I(s_0)\alpha + \mathcal{S}(1 - \alpha) \quad ,$$

also known as *alpha-blending*.

Alpha-blending has been introduced almost 30 years ago, and it is the *de facto* standard technique for transparency. Solving the rendering equation via alpha blending requires to handle object ordering, which means that if we want to correctly evaluate the rendering equation, we should assure that objects contribute to the final pixel color with the correct ordering. *Order-independent transparency* (OIT) denotes any technique that allows to render transparent objects without having to sort them before they are being rendered, thus sorting is performed by the technique itself (e.g. depth peeling (Everitt, 2001) and the A-Buffer (Carpenter, 1984)). OIT techniques are computationally intensive and complex. They often require extra efforts to be used with other techniques, e.g. antialiasing. For these reasons developers would avoid to implement OIT and would prefer a simpler and faster algorithm that does not require sorting. Of course, such techniques are non-physical, nevertheless sometimes they may still be sufficient to provide some insight into the data while avoiding the higher cost of a correct solution.

Bounded A-Buffer. The traditional image-based algorithm for fragment sorting is the Z-buffer (Catmull, 1974). However, for each pixel, only the fragment with the lowest (or greatest) depth is kept, and the others are discarded. The A-buffer (Carpenter, 1984) extends the Z-buffer by storing a list of rasterized fragments for each pixel, sorted by depth. Potentially, the A-buffer is a powerful tool to implement OIT techniques. Nevertheless, it requires an unbounded memory per pixel. Recently, Callahan et al. (2005) introduced the K-buffer, a per pixel fixed-size buffer of fragments that is maintained in GPU memory. There exist many proposals for implementing the K-Buffer on the GPU, for example by using the stencil routing algorithm (Myers & Bavoil, 2007) or by exploiting generic atomic operations available in OpenGL 4.0 (Yang et al., 2010). It requires only one geometric pass, thus being more efficient than techniques such as depth peeling (Everitt, 2001). Despite the technique can

store only K fragments per pixel, a recent extension called Adaptive Transparency overcomes this limitation by using an approximated and adaptively compressed visibility representation (Salvi et al., 2011).

Moreover, even the data types involved in transparency drastically change the effectiveness of the technique used (e.g. particle vs volumetric vs mesh). While each of the previously mentioned methods is a more or less straightforward mapping of the given data to a rendering method using shaders in OpenGL, fusing them into an integrated visualization encompassing more than one such type is non-trivial if transparency is involved.

Combining volume and particle visualization. Astrophysical simulations are a classical visualization scenario where often data of different types are involved. An example is having both particle-based and volumetric data. The approaches used to visualize transparent particle-based (e.g. splatting approaches, see Westover, 1990), and the ones used for volume, (e.g. texture-based slicing, see Weiler et al., 2000) or GPU-assisted ray casting (Kaehler et al., 2007; Kruger & Westermann, 2003) work well alone. Again, if we relax our needs and we consider one of the two data sets in input as completely opaque, we can afford a combined visualization by using a two pass approach: the first pass for opaque objects, and the second for transparent ones, thus we combine results by exploiting hardware depth-buffers and blending operations. Nevertheless, problems arise when both data sets are transparent. Kaehler et al. (2007) introduced an interesting approach for high-quality visualization of volume rendering of grid data and unstructured point set. Their approach is based on a GPU-accelerated raycasting algorithm, where point data is stored in a GPU-octree data structure (e.g. a 3d texture) in order to efficiently access it during ray traversal.

4. Results

4.1 Galaxy clusters

One main demand for a comprehensive data analysis is the visualization of both grid data (that comes from the hydrodynamical simulations) and the point data (coming from the N-body simulation and the SAM) at the same time. As expounded in the previous section, we are first and foremost interested in secondary effects of cosmic structure formation that influence the inter cluster medium. The analysis of the hydro-simulation should reveal, how material coming from galactic ram-pressure stripping and galactic winds behaves in this extremely hot ($10^7 - 10^9$ K) and thin (10^{-3} particles per cm^3) ICM.

The density and temperature plots in figures 4 (a) and (b) reveal crosswise major in-falling regions of hot gas that is further (shock-)heated and condensed in the central region of the cluster. The dots represent the galactic halos of which structures partially coincide with peaks in gas temperature and density, but clearly not always. This unique combined visualization of these two types of data reveals that groups of galaxy halos can produce remarkable substructures that also show in the gaseous component of the cluster. Furthermore there is a considerable amount of galaxies that are not fast enough to shock-heat the ICM excessively while descending towards the cluster center.

Especially fascinating in this context are the metallicity plots that disentangle chemical enrichment caused by galactic winds (Fig. 4 (c)) and ram-pressure stripping (Fig. 4 (d)). The trails of metals are much longer for the wind component and they begin much earlier in time and in further outwards regions of the cluster. Ram-pressure only acts above a certain

pressure threshold that can merely be achieved if both surrounding density of the ICM and the relative velocities of gas and galaxies are sufficient. Ram-pressure stripping however can in succession be especially effective and deprive the galaxy of a considerable fraction of its gas on cosmologically short time scales. Since galactic winds are predominantly driven by collective supernovae explosions as denoted in section 2.1.2, the metal yields are composed differently for wind respectively ram-pressure enriched material. This should lead to an inhomogeneous spatial distribution of chemical elements in a cluster which is however not yet observable with today's instruments and remains to be investigated also observationally in future projects.

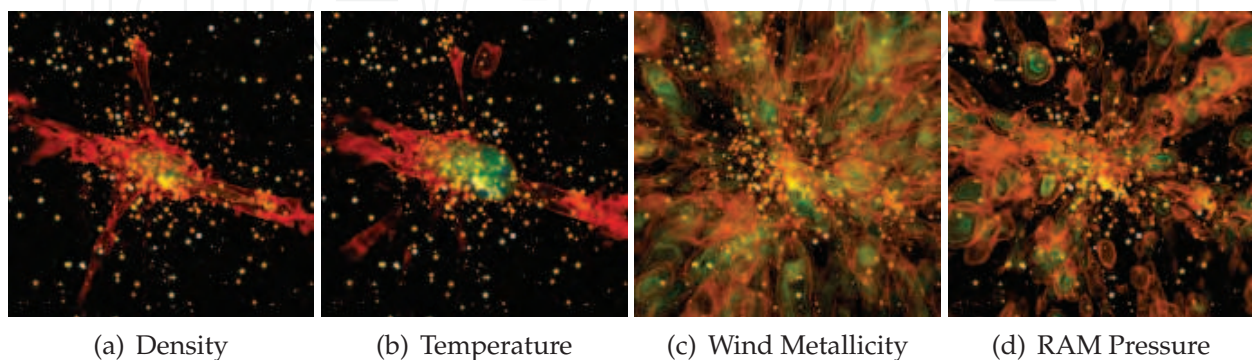


Fig. 4. Hydrodynamic quantities on the galaxy cluster.

4.2 Magnetic fields in clusters of galaxies

The technique outlined in section 3.4.2 is very well suited to investigate the correlations of plasma properties in the intra-cluster medium (ICM) from simulations of clusters of galaxies. The simulations cover the evolution of the intra-cluster medium (ICM) from an early redshift $z \sim 100$ to the present time ($z = 0$) and include cosmic expansion, dark matter, baryonic matter, magnetic fields, (magneto-) hydrodynamics and radiative cooling.

The correlations between certain plasma properties can give important information on the dynamics of the whole system that might not be detectable or quantifiable when looking at those properties separately. A good example for this is the correlation between the magnetic pressure p_{mag} and the density ρ in the ICM which gives an insight into the importance of turbulence and dynamo effects during the cluster creation. Fig. 5 shows a Dual Volume Rendering of magnetic pressure and density of the ICM for a cluster with a total mass of $M_{\text{tot}} = 2.72 \times 10^{14} M_{\odot}$ at redshift $z = 0$. In Fig. 5(d) the dense isocontours of the magnetic pressure together with the high density values (blue-green) but low density gradients clearly indicate a region with high magnetic turbulence, which is otherwise only visible in a $\log p_{\text{mag}} - \log \rho$ correlation diagram where features cannot be localized in the 3D domain. Likewise in Fig. 5(e), the purple region marks increased magnetic pressure caused by the inflow of matter into the center of the cluster. It is important to note that a high density does not necessarily correspond to a high magnetic pressure, as the blue colored density isocontours in Fig. 5(e) demonstrate.

We find that the Dual Volume Rendering technique is especially well suited for investigating correlations between plasma properties that are not obvious from the values alone, but also take into account the gradients of aforementioned properties. This visualization method

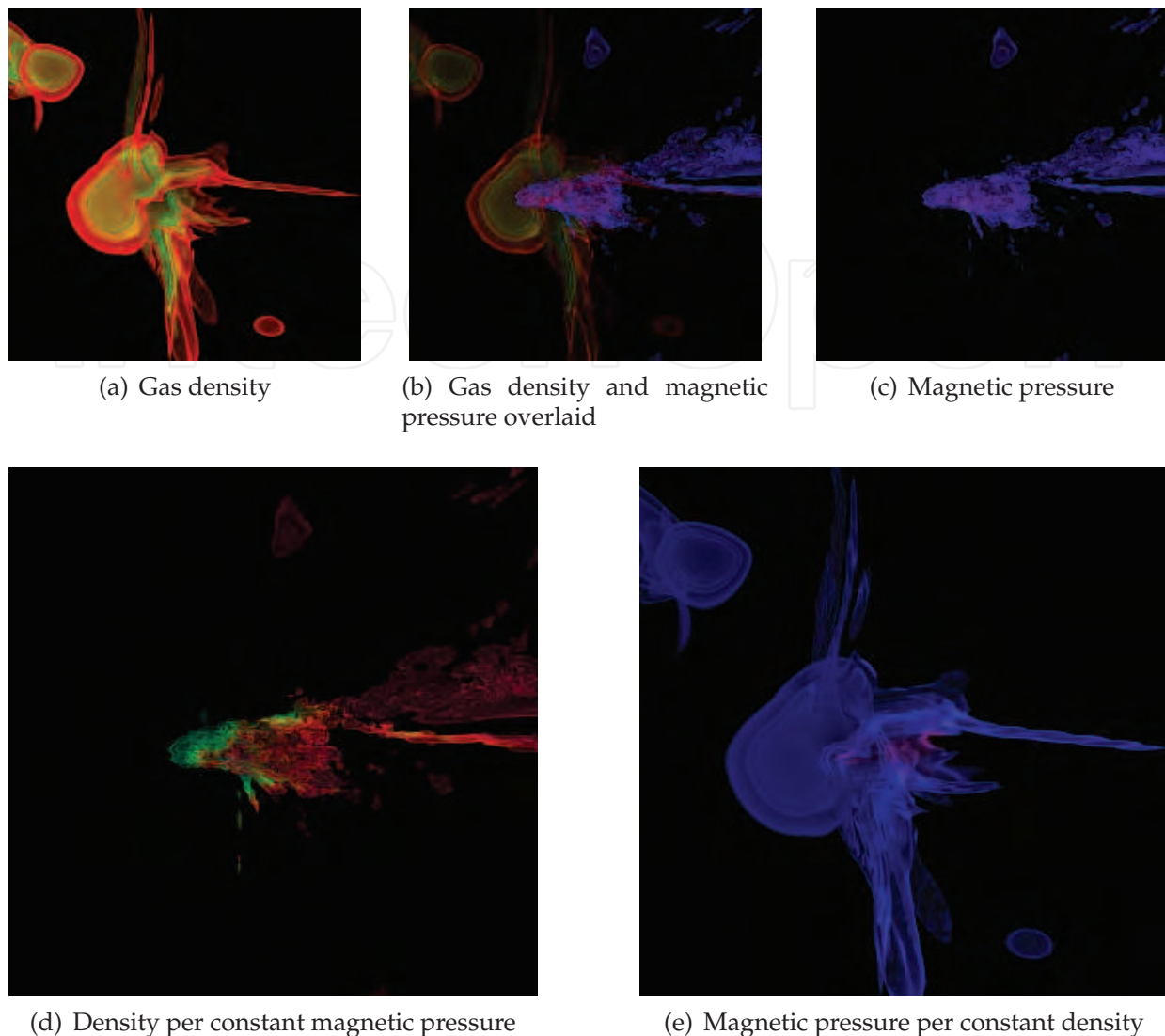


Fig. 5. Results from a MHD simulation of a cluster of galaxies at redshift $z = 0$. A classical volume rendering is shown in (a) to (c). The overlaid rendering (b) works very well to visualize the distribution of gas and the large scale structure of the magnetic field strength. In regions of rapid changing values or close to the highest concentrations of density and magnetic field strength however the overlaid plots conceal each other's features. This can be omitted by using Dual Volume Rendering, where one quantity is color mapped onto the isocontours of another quantity. In (d) the gas density (red - blue / low - high) is mapped onto the isobars of the magnetic field pressure, while in (e) the magnetic field pressure (blue - purple / low - high) is mapped onto the isocontours of the gas density.

allows to follow even steep gradients of both quantities that are being displayed together (compare (a) – (c) in Fig. 5 to the dual volume renderings (d) and (e)).

4.3 Ram-pressure stripping of disk galaxies

The simulations reveal many interesting results on ram-pressure stripped galaxies. The stripping of the gaseous disk is in well agreement with the Gunn & Gott criterion. The ram

pressure is calculated as $p_{\text{ram}} = \rho_{\text{ICM}} v_{\text{rel}}^2$. So, even low gas densities can deplete the gas mass in the disk if the relative velocity is higher. In the case of a high ram pressure, using a gas density of $10^{-27} \text{ g cm}^{-3}$ and a relative velocity of $v_{\text{rel}} = 1000 \text{ km s}^{-1}$, the gas disk is almost completely stripped.

Moreover, the simulations show that ram pressure enhances the star formation rate. In the previously described scenario, the star formation rate can be enhanced up to eight times compared to galaxies evolved in isolation. The reason can be found in the compression of the gas disk due to ram pressure and the formation of dense gas knots in the stripped gas wake of the galaxy. Also in these gas clumps stars are formed as already has been seen by (Kapferer et al., 2008). Hence, ram-pressure stripping can contribute to the intra-cluster stellar population (see e.g. Mihos et al., 2005).

Visualizations are crucial to study morphology and dynamics of the stripped ISM in detail. For this purpose, density plots and velocity fields of the different components of the model galaxies are shown in the following sections.

4.3.1 Scalar visualization

In Fig. 8 the density of the newly formed stars (bluish) and the ISM (reddish-greenish) is shown in a face-on (right) and edge-on view (left) for five different time steps. It can clearly be seen in the face on view that the gas disk gets compressed by ram pressure, with just a bunch of dense gas remaining in the disk. The stripping process first involves the outer parts of the gas disk which leads to a diffuse gas in the tail remaining at the starting point of the galaxy. From the inner parts of the spiral structured disk, a filamentary structure is formed in the wake which finally leads to the formation of the dense gas clumps, depicted in detail in Fig. 6 (b). These clumps are stable throughout a few hundred million years. In Fig. 6 (a) it is apparent, that the gas knots are affected by ram pressure as some gas gets stripped. Nevertheless, due to self-gravity and the pressure of the ICM, only a very small amount of gas is stripped and the gas loss is almost completely due to star formation. As can clearly be seen in Fig. 7, the new stars are formed in the dense gas clumps and are falling towards the disk as they do not feel the ram pressure anymore.

4.3.2 Vectorial visualization

A part from the morphology of the distribution of stars and gas, also the dynamic of these components is highly interesting. In Fig. 9, the method of Doppler Speckles is used to show the movement of the gas. From this plot, it is obvious that the angular momentum of the gas disk is being conserved also in the stripped gas tail. A detailed view is shown in Fig. 10. A differential movement of the gas can be seen. With respect to the galaxy itself, the gas knots in the wake are slowed down due to ram pressure. On the other hand it is very interesting that the gas knots themselves rotate as well as the filamentary dumbbell-like structure shows in Fig. 10 (b). This can explain the formation of the gas clumps. To this end, a detailed view on the dumbbell structure is shown in Fig. 11. The rotation of the filament leads to the formation of a gas clump at both ends. Furthermore, the part in between is more affected by ram pressure due to the lower density, hence it is pushed backwards with respect to the formed gas clumps. Finally, the two clumps are dismembered.

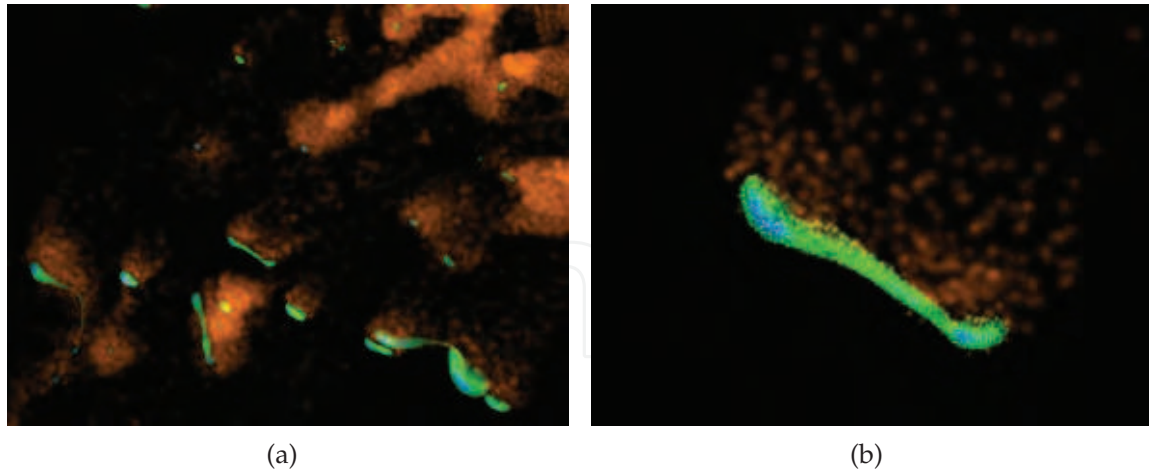


Fig. 6. Detail of high-density regions in the stripped gas tail.

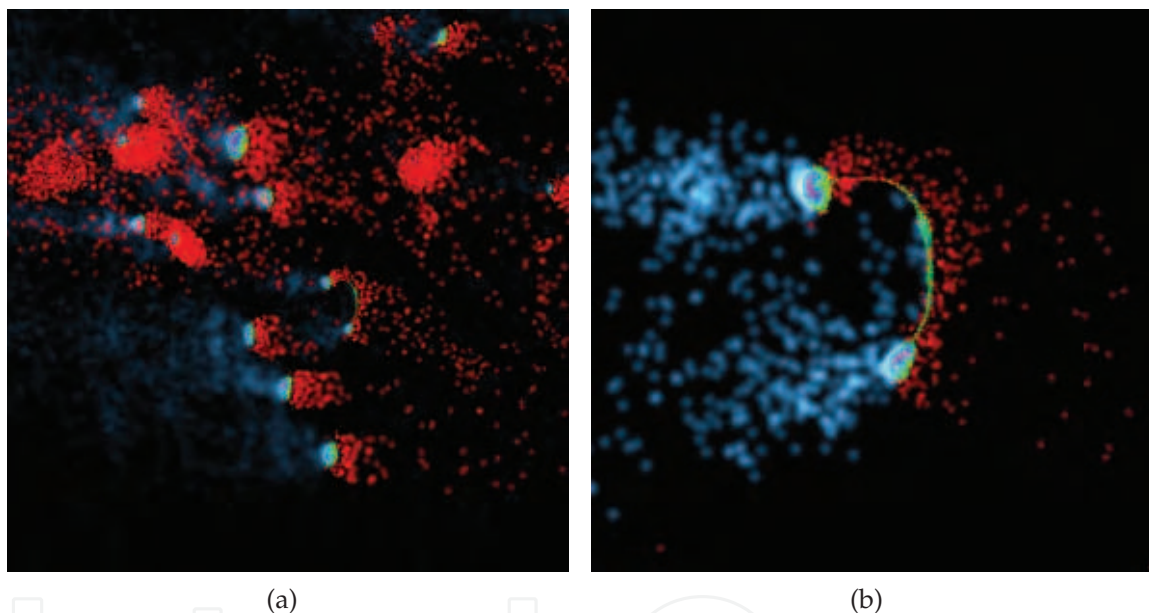


Fig. 7. Detail of star formation area and high-density regions

4.3.3 Tensorial visualization

Computing and visualizing the point distribution tensor allows to identify regions of predominantly linear, planar and isotropic distributions immediately.

4.4 Cosmological evolution

In a cosmological evolution of a galaxy cluster we simulated the behavior of dark matter from initial conditions up to presence. The simulation was performed using 2,097,152 particles. Of particular interest in cosmological simulations is the formation of voids, filaments and clusters of galaxies, as depicted in Fig. 14. While a slight elliptical shape of the central class can be glimpsed from the intensity distribution (Fig. 14(f)) the tensor display clearly depicts the anisotropy of the distribution (Fig. 14(g)).

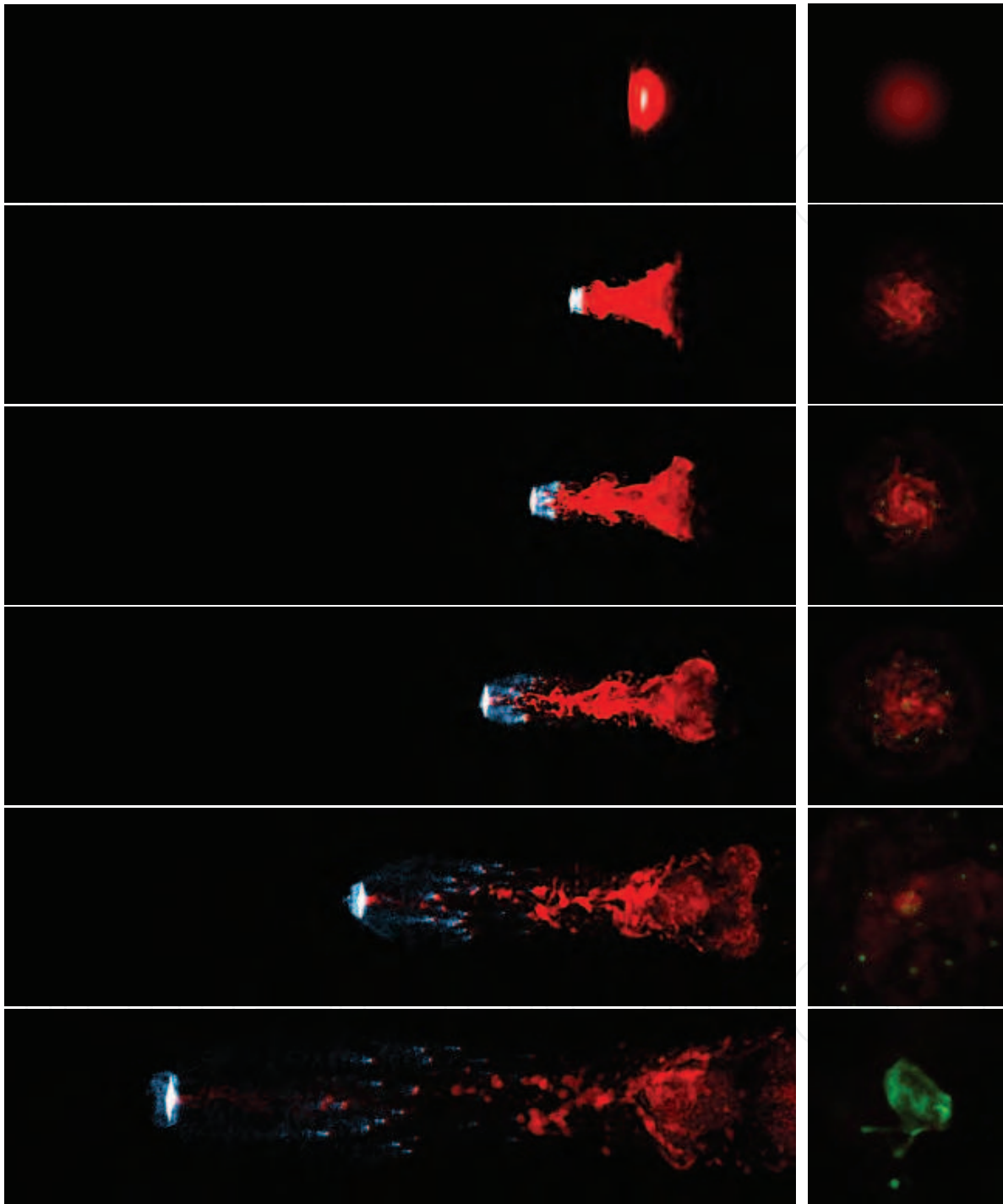


Fig. 8. Evolution of newly formed stars and gas for time steps $T=10,100,150,200,300$ and 400 Myr.

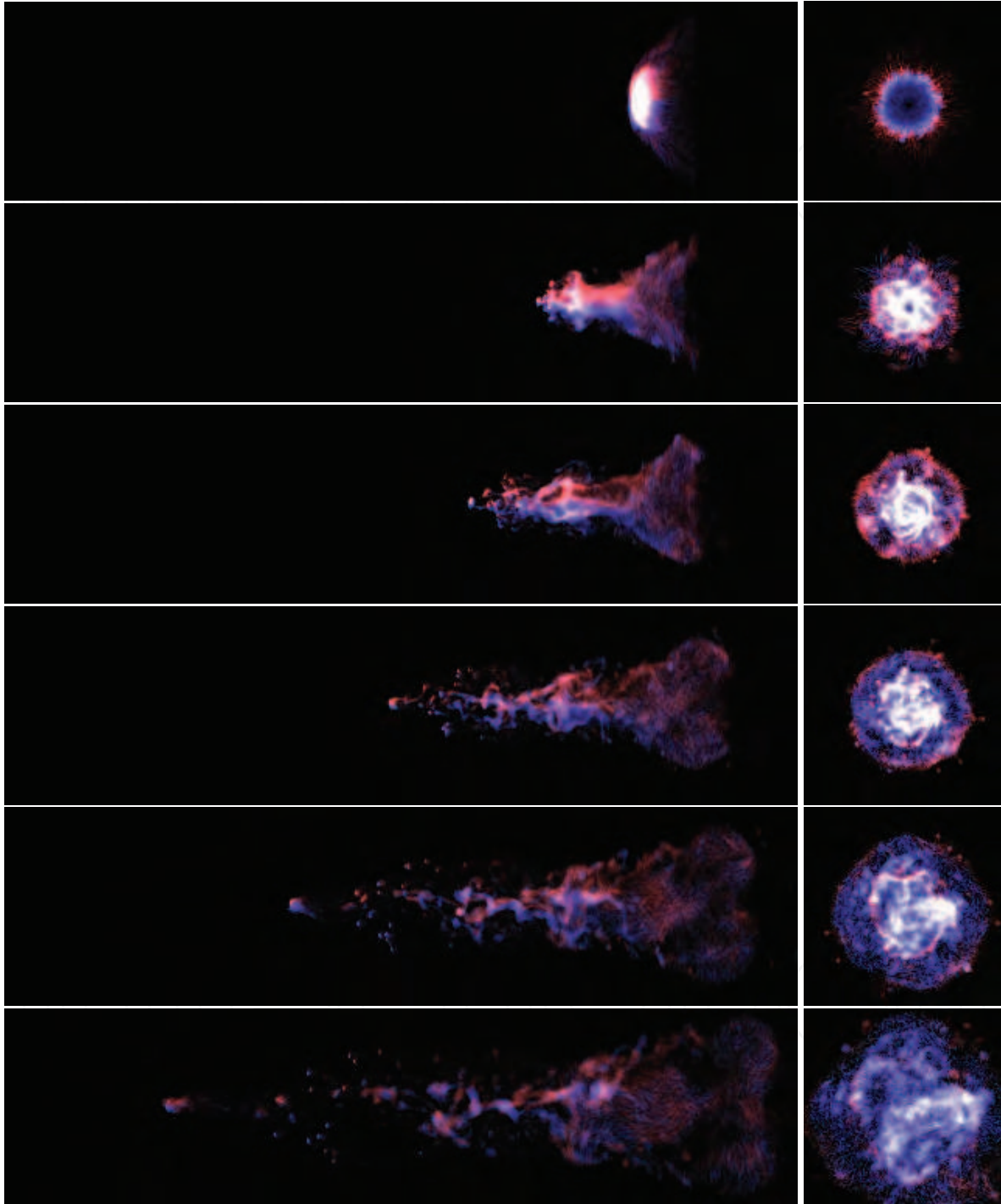


Fig. 9. Velocity of the gas, edge-on and front view for time steps $T=30,100,150,200,250$ and 300 Myr. Rendered using the method of Doppler Speckles.

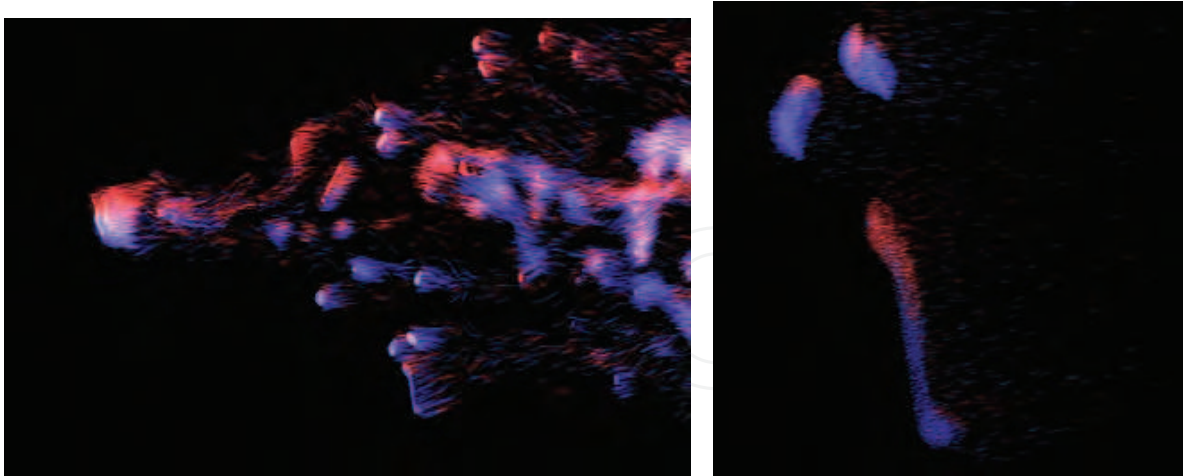


Fig. 10. Detail of velocity in high-density regions

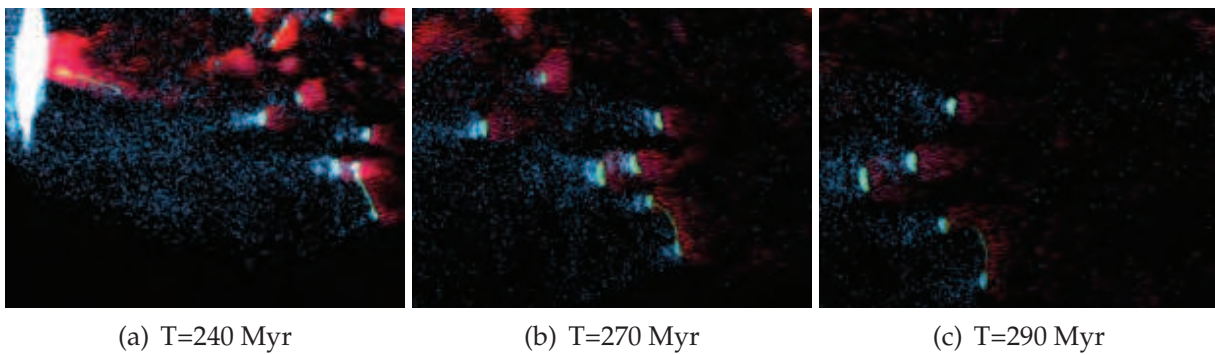


Fig. 11. Detailed evolution of a particular high-density region, showing velocity, density and newly formed stars.

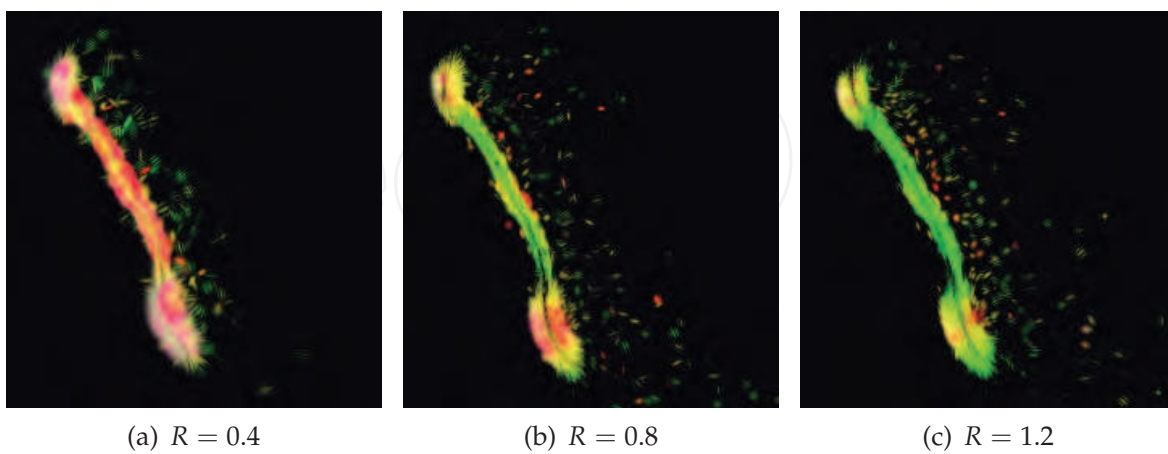


Fig. 12. Closeup of the dumbbell structure at $T = 25$ Myr. The images illustrate the influence of the radius of the chosen neighborhood on the resulting point distribution tensor. The geometric properties are best illustrated in (b) where the linear ribbon connects the two high density regions. If the radius is increased the whole dumbbell is becoming linear.

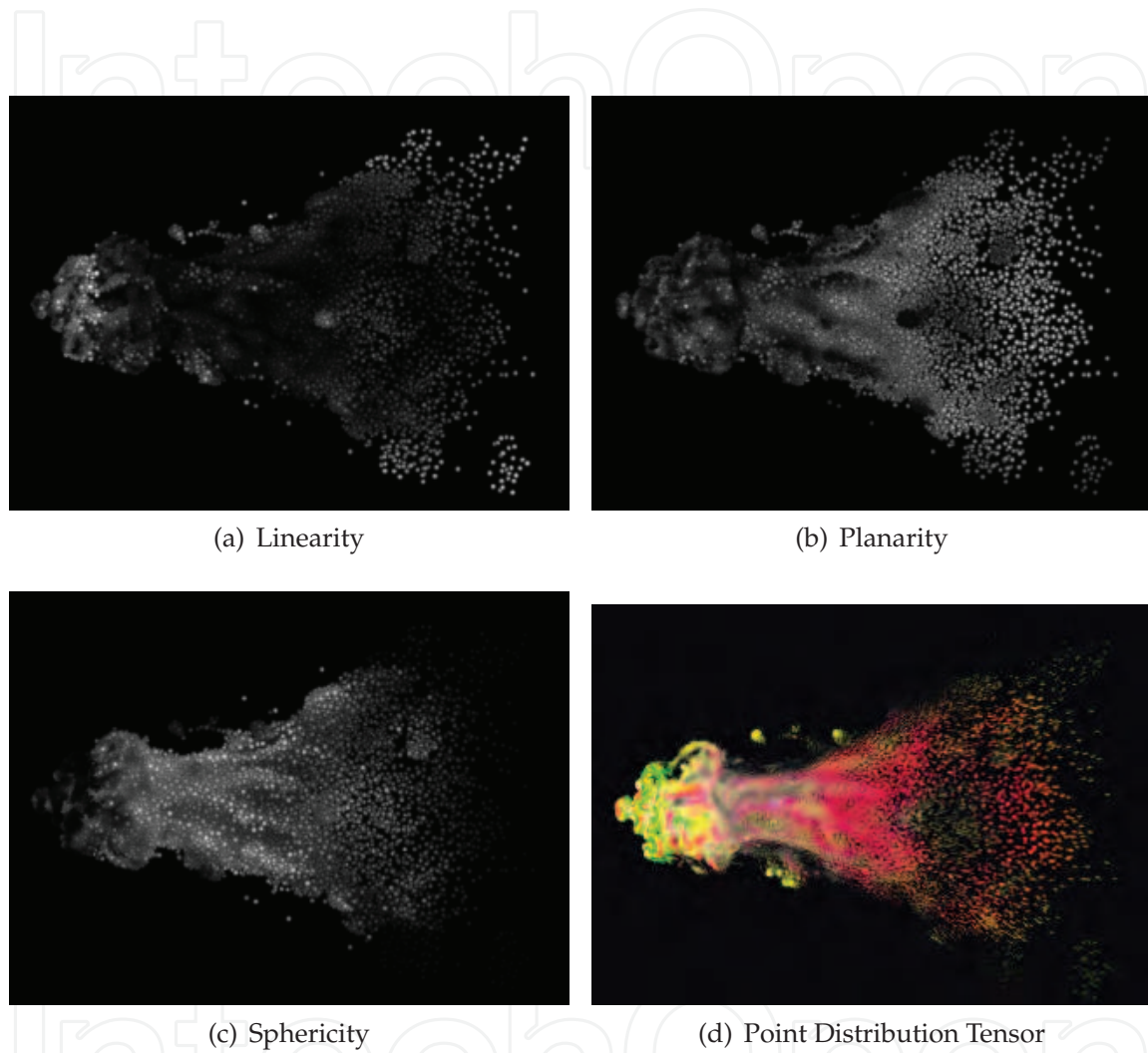
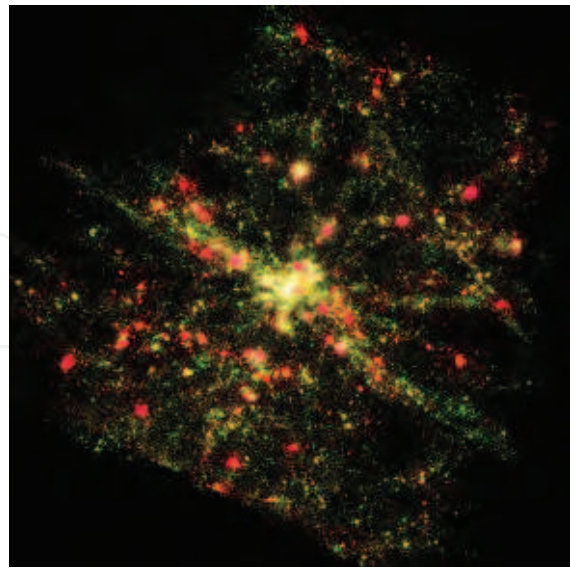


Fig. 13. Geometric properties of the gas particle distribution at $T = 10$ Myr. The 1280 nearest neighbors are selected for each particle. The distribution has a cone-like planar structure on the right side and forms a linear ring on the left. The greyscale scalar fields and the direct tensor splats illustrate these structures.



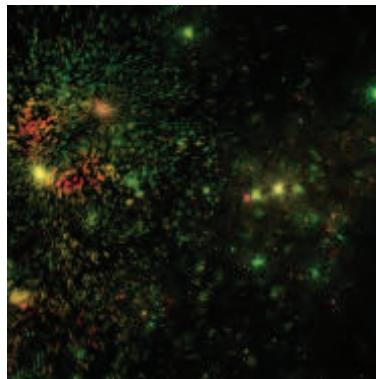
(a) Galaxy Distribution



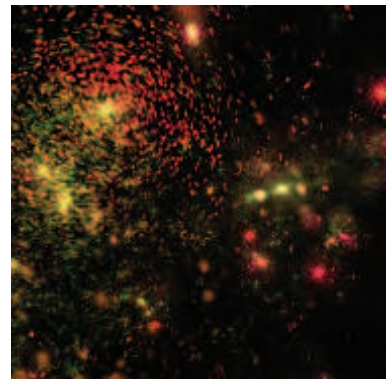
(b) Tensorial Galaxy Distance Analysis



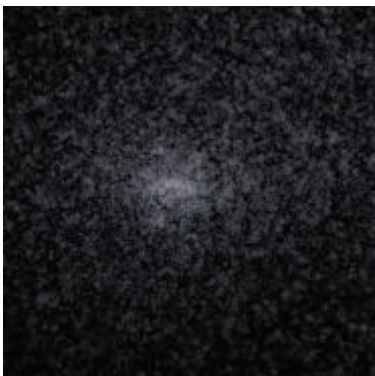
(c) Galaxie sub-cluster



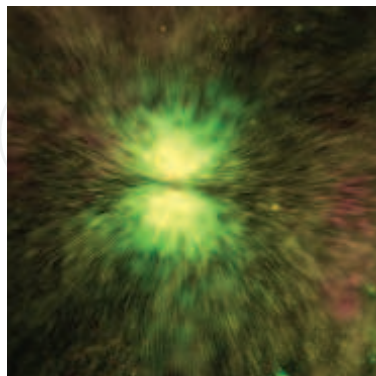
(d) Point distribution tensor of a sub-cluster



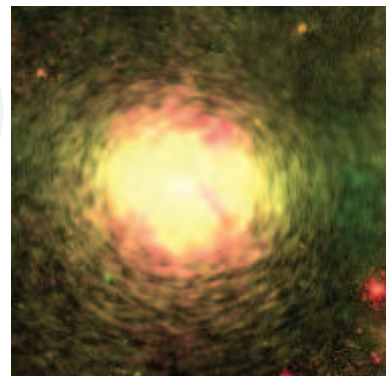
(e) Inverse point distribution tensor of a sub-cluster



(f) Locations in central cluster



(g) Point distribution tensor of central cluster



(h) Inverse point distribution tensor of central cluster

Fig. 14. Tensorial point distribution distance (2000 points considered for neighborhood computation) allows to recognize distribution features within a large volume of galaxies.

5. Conclusion

In this article we have presented a systematic way to study data sets from numerical astrophysics originating from simulations exploring open questions. We review a model to organize data for scientific visualization supporting high reusability of visualization algorithms by avoiding problem-specific data structures. This model is based on the mathematics of fiber bundles and we discuss the mapping of astrophysical simulation data sets into this framework. We investigate the available data fields in the fiber space, exploring scalar-, vector- and tensor- fields that are given or extractable from the given data sets. We also discussed how visualization techniques face the different challenges of these data sets, such as visualizing transparency of combined data sets and exploiting the computational power and new features available in current GPU hardware. Results include (magneto-) hydrodynamic quantities of galaxy cluster, ram-pressure stripped galaxies with scalar, vectorial and tensorial visualization, and cosmological evolution of galaxy cluster.

6. Acknowledgements

Part of this work was funded by *Austrian Science Foundation FWF DK+ project "Computational Interdisciplinary Modeling"* (W1227) and grant P19300. This research employed resources of the Center for Computation & Technology at Louisiana State University, which is supported by funding from the Louisiana legislature's Information Technology Initiative. This work was supported by the Austrian Ministry of Science BMWF as part of the UniInfrastrukturprogramm of the Forschungsplattform Scientific Computing at LFU Innsbruck.

7. References

- Andersson, J. (2010). Five Major Challenges in Interactive Rendering, ACM SIGGRAPH 2010 Beyond Programmable Shading Course.
- Barnes, J. & Hut, P. (1986). A hierarchical $O(N \log N)$ force-calculation algorithm, *Nature* 324: 446–449.
- Benger, W. (2004). *Visualization of General Relativistic Tensor Fields via a Fiber Bundle Data Model*, PhD thesis, FU Berlin.
URL: <http://www.lob.de/isbn/3865411088>
- Benger, W. (2008). Colliding galaxies, rotating neutron stars and merging black holes - visualising high dimensional data sets on arbitrary meshes, *New Journal of Physics* 10(12): 125004–+.
URL: <http://stacks.iop.org/1367-2630/10/125004>
- Benger, W. (2009). On safari in the file format djungle - why can't you visualize my data?, *Computing in Science & Engineering* 11(6): 98–102.
URL: http://www.computer.org/cms/Computer.org/ComputingNow/homepage/2009/1109/rW_CS_SafariFileFormatJungle.pdf
- Benger, W., Bartsch, H., Hege, H.-C., Kitzler, H., Shumilina, A. & Werner, A. (2006). Visualizing Neuronal Structures in the Human Brain via Diffusion Tensor MRI, *International Journal of Neuroscience* 116(4): pp. 461–514.
- Benger, W., Hamilton, A., Folk, M., Koziol, Q., Su, S., Schnetter, E., Ritter, M. & Ritter, G. (2010). Using geometric algebra for navigation in riemannian and hard disc space, in V. Skala & D. Hildebrand (eds), *GraVisMa 2009 - Computer Graphics, Vision and Mathematics*

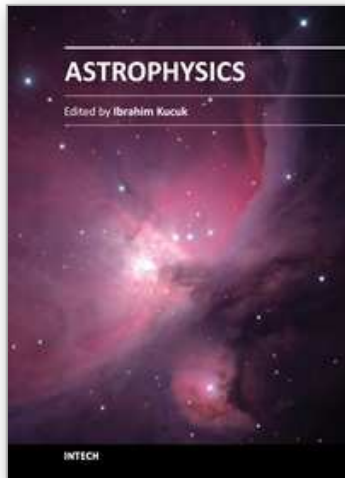
- for Scientific Computing*, UNION Agency, Na Mazinach 9, CZ 322 00 Plzen, Czech Republic.
URL: <http://gravisma.zcu.cz/GraVisMa-2009/>
- Benger, W. & Hege, H.-C. (2003). The tensor splats rendering technique, *Technical Report ZIB03-17*, Zuse Institute Berlin.
- Benger, W. & Hege, H.-C. (2006). *Strategies for Direct Visualization of Second-Rank Tensor Fields*, Springer, chapter 11, pp. 191–214.
URL: <http://www.springerlink.com/content/h264176262502825/>
- Benger, W., Heinzl, R., Hildenbrand, D., Weinkauff, T., Theisel, H. & Tschumperle, D. (2011). *Differential Methods for Multi-Dimensional Visual Data Analysis*, Springer Science + Business Media LLC, chapter 50, pp. 1533–1595.
URL: <http://www.springerlink.com/content/r4j504485j73jk16/>
- Benger, W., Ritter, G. & Heinzl, R. (2007). The Concepts of VISH, *4th High-End Visualization Workshop, Obergurgl, Tyrol, Austria, June 18-21, 2007*, Berlin, Lehmanns Media-LOB.de, pp. 26–39.
- Benger, W., Ritter, G., Su, S., Nikitopoulos, D. E., Walker, E., Acharya, S., Roy, S., Harhad, F. & Kapferer, W. (2009). Doppler speckles - a multi-purpose vectorfield visualization technique for arbitrary meshes, *CGVR'09 - The 2009 International Conference on Computer Graphics and Virtual Reality*.
- Benger, W. & Ritter, M. (2010). Using Geometric Algebra for Visualizing Integral Curves, in E. M. Hitzer & V. Skala (eds), *GraVisMa 2010 - Computer Graphics, Vision and Mathematics for Scientific Computing*, Union Agency - Science Press.
- Benson, A. J. (2010). Galacticus: A Semi-Analytic Model of Galaxy Formation, *ArXiv e-prints*.
- Berger, M. J. & Olinger, J. (1984). Adaptive mesh refinement for hyperbolic partial differential equations, *J. Comput. Phys.* 53: 484–512.
- Bertschinger, E. (1995). Cosmics: Cosmological initial conditions and microwave anisotropy codes.
- Bertschinger, E. (1998). Simulations of structure formation in the universe, *ANNUAL REVIEW OF ASTRONOMY AND ASTROPHYSICS* 36: 599–654.
- Blanton, E. L., Sarazin, C. L. & McNamara, B. R. (2003). Chandra Observation of the Cooling Flow Cluster Abell 2052, *The Astrophysical Journal* 585: 227–243.
- Butler, D. M. & Pendley, M. H. (1989). A visualization model based on the mathematics of fiber bundles, *Computers in Physics* 3(5): 45–51.
- Callahan, S. P., Ikits, M., Member, S., Comba, J. L. D. & Silva, C. T. (2005). Hardware-assisted visibility sorting for unstructured volume rendering, *IEEE Transactions on Visualization and Computer Graphics* 11: 2005.
- Carpenter, L. (1984). The a-buffer, an antialiased hidden surface method, *Proceedings of the 11th annual conference on Computer graphics and interactive techniques, SIGGRAPH '84*, ACM, New York, NY, USA, pp. 103–108.
URL: <http://doi.acm.org/10.1145/800031.808585>
- Catmull, E. E. (1974). *A Subdivision Algorithm for Computer Display of Curved Surfaces*, PhD thesis, Dept. of CS, U. of Utah.
- Chandrasekhar, S. (1960). *Radiative Transfer*, Dover Publications Inc.
- Crawfis, R. & Max, N. (1993). Textured splats for 3d scalar and vector field visualization, in Nielson & Bergeron (eds), *Visualization '93, San Jose*, IEEE CS Press, pp. 261–266.
- Cullip, T. J. & Neumann, U. (1994). Accelerating Volume Reconstruction With 3D Texture Hardware, *Technical report*, Chapel Hill, NC, USA.

- de Oliveira-Costa, A., Tegmark, M., Zaldarriaga, M. & Hamilton, A. (2004). Significance of the largest scale cmb fluctuations in wmap, *Phys. Rev. D* 69: 063516.
URL: <http://link.aps.org/doi/10.1103/PhysRevD.69.063516>
- Domainko, W., Kapferer, W., Mair, M., Schindler, S., Kampen, E. V., Kronberger, T., Moll, R., Kimeswenger, S., Ruffert, M. & Mangete, O. E. (2008). Metal Enrichment of the ICM due to Ram-Pressure Stripping of Cluster Galaxies, in B. Aschenbach, V. Burwitz, G. Hasinger, & B. Leibundgut (ed.), *Relativistic Astrophysics Legacy and Cosmology - Einstein's*, pp. 300–+.
- Dougherty, M. T., Folk, M. J., Bernstein, H. J., Bernstein, F. C., Eliceiri, K. W., Bengler, W., Zadok, E. & Best, C. (2009). Unifying biological image formats with hdf5, *Communications of the ACM* 52(10): 42–47.
- Everitt, C. (2001). Interactive order-independent transparency, *Technical report*, NVidia Technical Report.
- Finoguenov, A., David, L. P. & Ponman, T. J. (2000). An ASCA Study of the Heavy-Element Distribution in Clusters of Galaxies, *The Astrophysical Journal* 544: 188–203.
- Gingold, R. A. & Monaghan, J. J. (1977). Smoothed particle hydrodynamics - Theory and application to non-spherical stars, *mnras* 181: 375–389.
- Gunn, J. E. & Gott, III, J. R. (1972). On the Infall of Matter Into Clusters of Galaxies and Some Effects on Their Evolution, *apj* 176: 1–+.
- Hestenes, D. (1999). *New Foundations for Classical Mechanics, 2nd ed.*, Springer Verlag.
- Hester, J. A., Seibert, M., Neill, J. D., Wyder, T. K., Gil de Paz, A., Madore, B. F., Martin, D. C., Schiminovich, D. & Rich, R. M. (2010). IC 3418: Star Formation in a Turbulent Wake, *apj* 716: L14–L18.
- Kaehler, R., Abel, T. & Hege, H.-C. (2007). Simultaneous GPU-Assisted Raycasting of Unstructured Point Sets and Volumetric Grid Data , pp. 49–56.
URL: <http://www.eg.org/EG/DL/WS/VG/VG07/049-056.pdf>
- Kajiya, J. T. (1986). The rendering equation., *SIGGRAPH'86*, pp. 143–150.
- Kapferer, W., Kronberger, T., Ferrari, C., Riser, T. & Schindler, S. (2008). On the influence of ram-pressure stripping on interacting galaxies in clusters, *mnras* 389: 1405–1413.
- Kapferer, W., Sluka, C., Schindler, S., Ferrari, C. & Ziegler, B. (2009). The effect of ram pressure on the star formation, mass distribution and morphology of galaxies, *A&A* 499: 87–102.
- Katz, N., Weinberg, D. H. & Hernquist, L. (1996). Cosmological Simulations with TreeSPH, *apjs* 105: 19–+.
- Knebe, A., Knollmann, S. R., Muldrew, S. I., Pearce, F. R., Aragon-Calvo, M. A., Ascasibar, Y., Behroozi, P. S., Ceverino, D., Colombi, S., Diemand, J., Dolag, K., Falck, B. L., Fasel, P., Gardner, J., Gottlöber, S., Hsu, C.-H., Iannuzzi, F., Klypin, A., Lukić, Z., Maciejewski, M., McBride, C., Neyrinck, M. C., Planelles, S., Potter, D., Quilis, V., Rasera, Y., Read, J. I., Ricker, P. M., Roy, F., Springel, V., Stadel, J., Stinson, G., Sutter, P. M., Turchaninov, V., Tweed, D., Yepes, G. & Zemp, M. (2011). Haloes gone MAD: The Halo-Finder Comparison Project, *Monthly Notices of the Royal Astronomical Society* 415: 2293–2318.
- Kniss, J., Premoze, S., Hansen, C. & Ebert, D. (2002). Interactive Translucent Volume Rendering and Procedural Modeling, In *Proceedings of IEEE Visualization 2002*, pp. 109–116.

- Kronberger, T., Kapferer, W., Ferrari, C., Unterguggenberger, S. & Schindler, S. (2008). On the influence of ram-pressure stripping on the star formation of simulated spiral galaxies, *A&A* 481: 337–343.
- Kruger, J. & Westermann, R. (2003). Acceleration techniques for gpu-based volume rendering, *Proceedings of the 14th IEEE Visualization 2003 (VIS'03)*, VIS '03, IEEE Computer Society, Washington, DC, USA, pp. 38–.
- URL: <http://dx.doi.org/10.1109/VIS.2003.10001>
- Lorenzen, W. E. & Cline, H. E. (n.d.). Marching cubes: A high resolution 3d surface construction algorithm, *Computer Graphics* 21(4) 21(4): 163–169.
- Lovisari, L., Kapferer, W., Schindler, S. & Ferrari, C. (2009). Metallicity map of the galaxy cluster A3667, *Astronomy & Astrophysics* 508: 191–200.
- Lucy, L. B. (1977). A numerical approach to the testing of the fission hypothesis, *aj* 82: 1013–1024.
- Mihos, J. C., Harding, P., Feldmeier, J. & Morrison, H. (2005). Diffuse Light in the Virgo Cluster, *apj* 631: L41–L44.
- Mo, H. J., Mao, S. & White, S. D. M. (1998). The formation of galactic discs, *mnras* 295: 319–336.
- Monaghan, J. J. & Lattanzio, J. C. (1985). A refined particle method for astrophysical problems, *Astronomy & Astrophysics* 149: 135–143.
- Myers, K. & Bavoil, L. (2007). Stencil Routed K-Buffer, *Technical report*, NVidia Technical Report.
- Navarro, J. F., Frenk, C. S. & White, S. D. M. (1996). The Structure of Cold Dark Matter Halos, *apj* 462: 563–+.
- Ostriker, J. & Steinhardt, P. J. (1995). Cosmic concordance.
- Ritter, M. (2011). *Geodesics in Numerical Space Times*, Verlag Dr. Müller.
- Salpeter, E. E. (1955). The Luminosity Function and Stellar Evolution., *apj* 121: 161–+.
- Salvi, M., Montgomery, J. & Lefohn, A. (2011). Adaptive transparency, *Proceedings of the ACM SIGGRAPH Symposium on High Performance Graphics*, HPG '11, ACM, New York, NY, USA, pp. 119–126.
- URL: <http://doi.acm.org/10.1145/2018323.2018342>
- Springel, V. (2005). The cosmological simulation code GADGET-2, *Monthly Notices of the Royal Astronomical Society* 364: 1105–1134.
- Springel, V. & Hernquist, L. (2003). Cosmological smoothed particle hydrodynamics simulations: a hybrid multiphase model for star formation, *mnras* 339: 289–311.
- Stöckl, J., Steinhauser, D., Haider, M. & Riser, T. (2010). Improved visualisation of 3d volumetric datathrough pointwise phong shading based on normal mapping, in W. Benger, A. Gerndt, S. Su, W. Shoor, M. Koppitz, W. Kapferer, H. P. Bischof & M. Di Pierro (eds), *Proceedings of the 6th High-End Visualization Workshop*, Vol. 6 of *Proceedings of the High-End Visualization Workshop*, Lehmanns Media, Berlin, 2010, pp. 107–121.
- Treinish, L. A. (1997). Data explorer data model, http://www.research.ibm.com/people/l/1loydt/dm/dx/dx_dm.htm.
- van Kampen, E., Jimenez, R. & Peacock, J. A. (1999). Overmerging and mass-to-light ratios in phenomenological galaxy formation models, *Monthly Notices of the Royal Astronomical Society* 310: 43–56.
- Weiler, M., Westermann, R., Hansen, C., Zimmermann, K. & Ertl, T. (2000). Level-of-detail volume rendering via 3d textures, *Proceedings of the 2000 IEEE symposium on Volume*

- visualization*, VVS '00, ACM, New York, NY, USA, pp. 7–13.
URL: <http://doi.acm.org/10.1145/353888.353889>
- Westin, C., Peled, S., Gudbjartsson, H., Kikinis, R. & Jolesz, F. (1997). Geometrical diffusion measures for mri from tensor basis analysis, *Proceedings of ISMRM, Fifth Meeting, Vancouver, Canada*, p. 1742.
URL: <http://spl.bwh.harvard.edu:8000/pages/ppl/westin/papers/smr97/htmlversion.html>
- Westover, L. (1990). Footprint evaluation for volume rendering, *Proceedings of the 17th annual conference on Computer graphics and interactive techniques*, ACM Press, NY, USA, pp. 367–376.
- White, S. D. M. & Frenk, C. S. (1991). Galaxy formation through hierarchical clustering, *The Astrophysical Journal* 379: 52–79.
- Yang, J. C., Hensley, J., Grün, H. & Thibieroz, N. (2010). Real-time concurrent linked list construction on the gpu, *Computer Graphics Forum* 29(4): 1297–1304.

IntechOpen



Astrophysics

Edited by Prof. Ibrahim Kucuk

ISBN 978-953-51-0473-5

Hard cover, 398 pages

Publisher InTech

Published online 30, March, 2012

Published in print edition March, 2012

This book provides readers with a clear progress to theoretical and observational astrophysics. It is not surprising that astrophysics is continually growing because very sophisticated telescopes are being developed and they bring the universe closer and make it accessible. Astrophysics Book presents a unique opportunity for readers to demonstrate processes do occur in Nature. The unique feature of this book is to cover different aspects in astrophysics covering the topics: • Astronomy • Theoretical Astrophysics • Observational Astrophysics • Cosmology • The Solar System • Stars • Planets • Galaxies • Observation • Spectroscopy • Dark Matter • Neutron Stars • High Energy Astrophysics

How to reference

In order to correctly reference this scholarly work, feel free to copy and paste the following:

Werner Benger, Markus Haider, Harald Höller, Dominik Steinhauser, Josef Stöckl, Biagio Cosenza and Marcel Ritter (2012). Visualization Methods for Numerical Astrophysics, Astrophysics, Prof. Ibrahim Kucuk (Ed.), ISBN: 978-953-51-0473-5, InTech, Available from: <http://www.intechopen.com/books/astrophysics/visualization-methods-for-numerical-astrophysics>

INTECH
open science | open minds

InTech Europe

University Campus STeP Ri
Slavka Krautzeka 83/A
51000 Rijeka, Croatia
Phone: +385 (51) 770 447
Fax: +385 (51) 686 166
www.intechopen.com

InTech China

Unit 405, Office Block, Hotel Equatorial Shanghai
No.65, Yan An Road (West), Shanghai, 200040, China
中国上海市延安西路65号上海国际贵都大饭店办公楼405单元
Phone: +86-21-62489820
Fax: +86-21-62489821

© 2012 The Author(s). Licensee IntechOpen. This is an open access article distributed under the terms of the [Creative Commons Attribution 3.0 License](#), which permits unrestricted use, distribution, and reproduction in any medium, provided the original work is properly cited.

IntechOpen

IntechOpen